Crystal Structures of HIV-1 Reverse Transcriptase with Etravirine (TMC125) and Rilpivirine (TMC278): Implications for Drug Design[†]

Eric B. Lansdon,* Katherine M. Brendza, Magdeleine Hung, Ruth Wang, Susmith Mukund,[‡] Debi Jin, Gabriel Birkus, Nilima Kutty, and Xiaohong Liu

Gilead Sciences, Inc., 333 Lakeside Drive, Foster City, California 94404. [‡]*Current Address: Department of Protein Crystallography, Genentech, 1 DNA Way, South San Francisco, California 94080.*

Diarylpyrimidine (DAPY) non-nucleoside reverse transcriptase inhibitors (NNRTIs) have inherent flexibility, helping to maintain activity against a wide range of resistance mutations. Crystal structures were determined with wild-type and K103N HIV-1 reverse transcriptase with etravirine (TMC125) and rilpivirine (TMC278). These structures reveal a similar binding mode for TMC125 and TMC278, whether bound to wild-type or K103N RT. Comparison to previously published structures reveals differences in binding modes for TMC125 and differences in protein conformation for TMC278.

Introduction

HIV-1 reverse transcriptase (RT[a]) performs an integral part of HIV-1 virus replication and is a major target for antiretroviral therapies. There are currently two classes of RT inhibitors used in clinical treatment. Nucleoside and nucleotide reverse transcriptase inhibitors (NRTIs) compete with the natural dNTP at the polymerase active site, acting as chain terminators preventing further polymerization. Second, non-nucleoside reverse transcriptase inhibitors (NNRTI) bind approximately 10 Å from the polymerase active site, disrupting RT polymerase function allosterically.[1] Both classes of RT inhibitors are critical components of HAART (highly active antiretroviral therapy) for the treatment of HIV infection. Despite the success of combination therapy, the emergence of drug resistance is still problematic. Thus, the development of new NNRTIs with improved resistance profiles continues to be an active area of research.

The non-nucleoside inhibitor-binding pocket (NNIBP) resides in the palm domain of RT, an especially flexible portion of the protein. Though NNRTIs represent a diverse structural class of compounds (Figure 1), they bind to the NNIBP with many common features. Early NNRTIs relied heavily on π-stacking interactions to Y181 and Y188, which can easily mutate, conferring resistance. New NNRTIs endeavored to reduce these interactions, relying more on W229 for example, which is less prone to mutation. Importantly, a common feature of newer NNRTIs is the addition of a central hydrogen bond to the backbone carbonyl of Lys101.

There are currently four approved drugs that target the NNIBP. Delavirdine and nevirapine are considered first generation NNRTIs and show a dramatic loss of activity with single point mutations in the NNIBP. Efavirenz is effective against many point mutations; however, efficacy is strongly compromised by the K103N mutation. K103N is the most prevalent NNRTI resistance-associated mutation. In recent studies, it has been observed in nearly 57% of NNRTI-resistant HIV-1 clinical isolates.[2,3] Tibotec Pharmaceuticals, Ltd. developed etravirine (TMC125), and it is now marketed by Tibotec Therapeutics, a division of Ortho Biotech Products, L.P. under the brand name Intelence.[4] TMC125 recently attained accelerated/conditional approved for use in treatment-experienced adult patients. Rilpivirine (TMC278) is currently under development by Tibotec Pharmaceuticals, Ltd. and has progressed into late stage clinical trials.[5−7] TMC125 and TMC278 are diarylpyrimidine (DAPY) NNRTIs with high activity against wild-type and mutant virus strains including K103N.[4,6,8] A design feature for these compounds is the innate flexibility between aromatic rings, allowing the compound to adopt multiple conformations, and is one explanation for the potent activity against many resistant virus strains.[9]

Rational design of new NNRTIs is challenging because of the plasticity of the NNIBP, and thus, structural changes related to compound binding are difficult to predict on the basis of current computational methods. Consequently, this highlights the importance of obtaining high-quality experimental data on the binding of NNRTIs. The ability to obtain structural data for RT with TMC125 or TMC278 may be hampered by the conformational flexibility of the compounds. Prior cocrystal structures reported in the DAPY series were of wild-type RT with TMC120 and R185545, mutant K103N RT with TMC125,[9] and recently, cocrystal structures of wild-type and mutant RT with TMC278.[10] However, to obtain the crystal structures with TMC278, a mutant RT was engineered that more readily crystallized with TMC278.[10,11] The purpose of this study was to obtain crystal structures of DAPY NNRTIs with a more physiological form of RT. Crystal structures of wild-type and K103N HIV-1 RT in complexes with TMC125 and TMC278 are reported here.

Results

To obtain cocrystals with TMC125 and TMC278, a crystal seeding strategy was employed using previously grown cocrystals of RT with nevirapine as seeds to obtain new cocrystals with TMC125 or TMC278 (Experimental Section). The cocrystals with the respective DAPY compounds were then used as seeds in another round of cocrystallization to ensure that the initial nevirapine cocrystals were insignificant by mass and not biasing structure determination. Table 1 lists data collection and refinement statistics.

Structures of Wild-Type and K103N RT with TMC125. Because of the limited structural information for TMC125 binding to RT, our goal was to provide insight into the potent activity of TMC125 against RT through structural investigation. TMC125 is bound with the central pyrimidine ring positioned between L100 and V179 (Figure 2A). The primary amine and bromo substituents point toward an opening in the pocket between K101 on the p66 subunit and E138 of the p51 subunit. Many next generation NNRTIs rely on a key hydrogen bond interaction between the K101 and
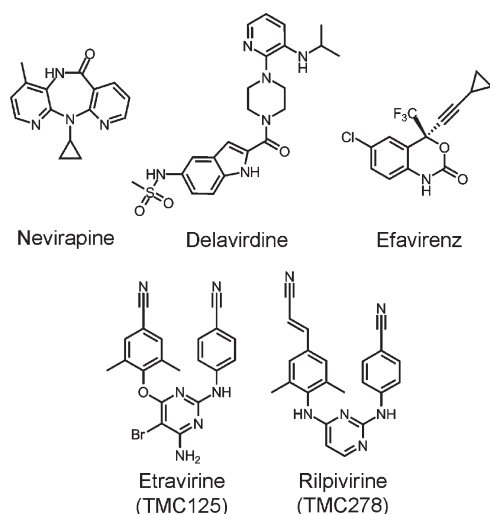

Figure 1. Chemical structures of selected NNRTIs.

the inhibitor. This conserved hydrogen bond (2.6 Å) is also observed in TMC125. The benzonitrile is positioned in a pocket defined by V106, P225, P236, F227, Y318, and L234. The linear nitrile group is positioned among the side chain of F227 and the backbone of H235 and P236. K103 has strong electron density for the entire side chain and lies below the pyrimidine and benzonitrile rings. No polar interactions are observed for the side chain to TMC125; however, possible contributions to binding of TMC125 are made via van der Waals interactions which have previously been hypothesized to aid in the binding of efavirenz in this region of the pocket.[12]

The dimethylcyanophenyl substituent is positioned toward the subpocket lined with the aromatic side chains Y188, W229, and F227. The *p*-cyano group is located in a hydrophobic area between the W229 and F227 side chains. Both cyano groups of TMC125 lie on either side of F227, forming the prototypical horseshoe shape observed in the crystal structure of wild-type RT with TMC120 and R185545.[9]

In the previously reported structure of K103N RT with TMC125, the DAPY compound did not form the anticipated horseshoe shape, displaying the ether linked dimethylcyanophenyl in an up position across Y181 and Y188 (see Discussion). Given that the horseshoe shape is observed in this wild-type RT structure, we decided to additionally determine the structure of the K103N mutant RT with TMC125 using the same crystallization method (Figure 2B). With the K103N RT mutation, the horseshoe conformation of TMC125 is maintained as observed in the wild-type structure. Consistent with the wild-type structure, the conserved hydrogen bond between the secondary amine and K101 backbone carbonyl (2.7 Å) is present. The N103 side chain sits below TMC125, and the NH_2 or O is within 3.3 Å of the secondary amine (the amide conformation is ambiguous). The lack of structural diversity between wild-type and K103N RT is consistent with other reports of the K103N mutation where no changes in compound binding was observed compared to wild-type RT.[12,13]

Structures of Wild-Type and K103N RT with TMC278. Because of the documented difficulty in obtaining cocrystal structures with TMC278, we felt that employing similar methods as with TMC125 might lead to structures with TMC278. Indeed, structures were determined with wild-type
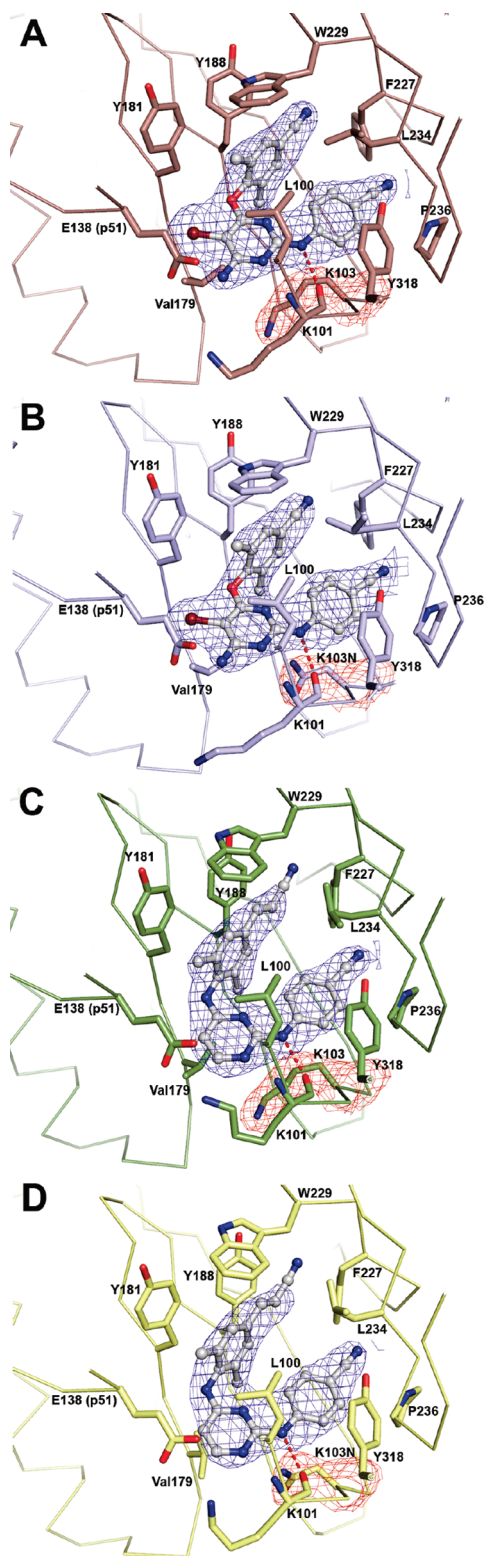
Table 1. X-ray Data Collection and Refinement Statistics

	WT-TMC125	K103N-TMC125	WT-TMC278	K103N-TMC278
		Data Collection		
X-ray source	ALS BL5.0.1	ALS BL5.0.2	ALS BL5.0.1	ALS BL5.0.1
wavelength (Å)	0.98	1.00	0.98	0.98
unit cell (*a, b, c* in Å)[a]	119.0, 154.1, 154.8	119.6, 154.0, 153.5	119.6, 155.0, 153.5	119.6, 154.9, 153.7
resolution (Å)	50.0−2.3 (2.34−2.3)	50.0−2.5 (2.55−2.50)	50.0−2.4 (2.45−2.40)	50−2.8 (2.85−2.80)
no. of reflections	282 264	196 934	209 187	138 388
no. unique	62 068	46 069	54 926	33 790
I/σ	17.1 (3.6)	21.2 (3.6)	15.9 (2.8)	17.0 (3.0)
R_{merge}[b] (%)	5.8 (44.3)	5.3 (47.7)	5.9 (46.9)	6.2 (50.8)
completeness (%)	99.2 (99.5)	94.0 (92.6)	98.2 (98.0)	94.9 (91.3)
		Refinement Statistics		
resolution (Å)	30.0−2.3	30.0−2.5	30.0−2.4	30.0−2.8
no. reflections ($F \geq 0$)	57 048	42 705	49 305	30 432
R-factor[c]	22.6	22.4	22.2	22.9
R_{free}[c]	27.0	27.7	26.1	28.9
rms bond lengths (Å)	0.008	0.008	0.008	0.009
rms bond angles (deg)	1.1	1.2	1.1	1.2

[a] All crystals belong to space group *C*222$_1$. [b] $R_{merge} = [\sum_h \sum_i |I_h - I_{hi}| / \sum_h \sum_i I_{hi}]$ where I_h is the mean of I_{hi} observations of reflection *h*. Numbers in parentheses represent highest resolution shell. [c] *R*-factor and $R_{free} = \sum ||F_{obs}| - |F_{calc}|| / \sum |F_{obs}| \times 100$ for 95% of recorded data (*R*-factor) or 5% of data (R_{free}).

Figure 2. Cocrystal structures of (A) HIV-1 RT with WT-TMC125, (B) K103N-TMC125, (C) WT-TMC278, and (D) K103N-TMC278. Shown in blue mesh and contoured at 1.0σ is the composite omit map drawn around the inhibitor. The omit map for the K103(N) side chain is shown in red mesh. The hydrogen bond between the secondary amine and the main chain carbonyl of Lys101 is illustrated with a dashed line. All structure figures were generated by Pymol (www.pymol.org).

RT and TMC278 without modification of our cocrystallization approach (Figure 2C). The inhibitor is positioned in a similar fashion as TMC125 in the NNIBP, adopting the expected horseshoe type shape. The pyrimidine ring of TMC278 is situated between V179 and L100 in the NNIBP with the secondary amine making the conserved hydrogen bond with K101 (2.7 Å). As noted in the wild-type TMC125 structure, the K103 side chain is well ordered and is located below the benzonitrile and pyrimidine rings. The dimethyl-phenylacrylonitrile group sits across Tyr181 and Tyr188 side chains. The electron density for the acrylonitrile drops off toward the end of the group, consistent with an increase in temperature factors for these atoms compared to the better positioned aromatic rings of TMC278. As previously observed, the acrylonitrile protrudes through a hydrophobic opening formed by residues W229, Y188, F227, and L234.[10]

TMC278 was also cocrystallized with K103N RT to gain insight into the nature of retained activity against this important resistance mutation (Figure 2D). The position of TMC278 in the pocket reveals no evidence of shifting in response to the K103N mutation. N103 sits below TMC278, and the amide forms a long-range hydrogen bond to the secondary amine linker (3.1 Å) and the carbonyl of K101 (3.0 Å).

Comparison of TMC125 and TMC278 Binding Modes with RT. The flexible linkers connecting aromatic rings in the DAPY compounds allow for the possibility of many conformations; however, the inhibitors in the structures here adopt very similar positions in the NNIBP (Figure 3). Table 2 lists the torsion angles among the aromatic rings in these structures. Because of the lack of substituents, the pyrimidine ring of TMC278 slides closer to E138 (p51) than observed with TMC125 (from 4.3 to 3.8 Å). Given the adjusted position of the TMC125 pyrimidine in the pocket, the benzonitrile is shifted closer to the protein backbone near V234. The main differences in protein conformation are observed in sheets β12−β13−β14. The cyano group in TMC125 pushes further toward H235 and P236, resulting in the β13−β14 loop projecting from the NNIBP more than what is observed for TMC278.

The interactions with Y181 and Y188 are also somewhat different between TMC125 and TMC278. The larger dimethylphenylacrylonitrile group of TMC278 interacts with Y181 and Y188 more than the dimethylcyanophenyl or TMC125. Notably, the acrylonitrile of TMC278 protrudes further into the pocket formed between W229 and F227. As such, the β12 sheet is shifted to allow the acrylonitrile group to position among these two side chains.

Discussion

The difficulty of generating cocrystal structures of RT with TMC125 and TMC278 has been reported several times.[9−11] There has been one previously reported structure of the K103N resistance mutation with TMC125, PDB code 1SV5.[9] Significant differences exist between the structures reported here for TMC125 and the previously published structure which is highlighted by a rmsd of 1.1 Å between K103N RT structures (Figure 4A). The conserved hydrogen bond between TMC125 and K101 carbonyl is not maintained in 1SV5, although there is a hydrogen bond (2.7 Å) to the carbonyl of K102. The binding mode of TMC125 in 1SV5 brings the primary amine within 2.4 Å of the main chain nitrogens of K102 and K103. Another major difference between the structures is the position of the dimethylcyanophenyl group. In 1SV5, this pendent group is pointed up between Y181 and Y188, in contrast to the structure reported here, where this ring lies across these aromatic residues,
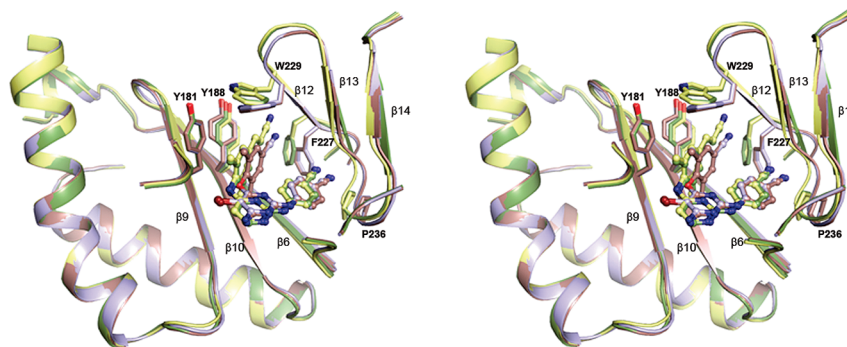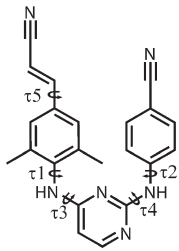
Figure 3. Stereodiagram showing the comparison of the four RT structures with TMC125 and TMC278. The color scheme is the same as Figure 2. All alignments were created by superimposing Cα atoms from residues 94−118, 156−215, 225−243, and 317−319 of the p66 subunit and 137−139 of the p51 subunit. Only residues that were used in the superposition are shown with the exception of 94−100 which were removed to give an unobstructed view of the binding pocket.

Table 2. Torsion Angles (deg) of TMC125 and TMC278 When Bound to RT

	τ1	τ2	τ3	τ4	τ5
WT-TMC125	−95	16	−13	−2	
K103N-TMC125	−91	22	−18	−1	
WT-TMC278	−96	0	−21	−1	180
K103N-TMC278	−97	0	−20	−1	179

forming the typical horseshoe shape. The crystal structures of wild-type RT with TMC120 (PDB code 1S6Q) and R185545 (PDB code 1SUQ) are more similar to the structures of TMC125 presented here. TMC120 and R185545 adopt the more recognizable horseshoe conformation and have protein rmsd values between 0.5 and 0.7 Å when compared to the wild-type structure of TMC125.

Direct comparison of the cocrystal structures of RT with TMC278 reveals differences in protein conformation (Figure 4B). By alignment of the protein backbone Cα's from 110 residues in the NNIBP, the rmsd among wild-type RT with TMC278 presented here and the published structures 2ZD1, 3BGR, and 2ZE2 varies from 1.1 to 1.2 Å. Despite the large rmsd, the overall position and torsion of the pendent groups do not vary dramatically for TMC278, which suggests that TMC278 can bind to different conformations of the NNIBP such as conformations resulting from resistance mutations within the pocket. The main difference observed in conformation of TMC278 is the orientation of the acrylonitrile. In the structures presented here, the acrylonitrile is pointed "down" (relative to Y188) compared to the "up" position observed in the three previously reported structures. This difference in the position of the acrylonitrile possibly leads to differences observed with the protein itself. Sheets β9−β10 show a significant change that is most prominent at the connector loop. As shown in Figure 4B, the position of Y183 between the two wild-type structures varies. This large shift in Y183 may be due to the acrylonitrile turned into the "up" position, allowing for more extensive interaction with the side
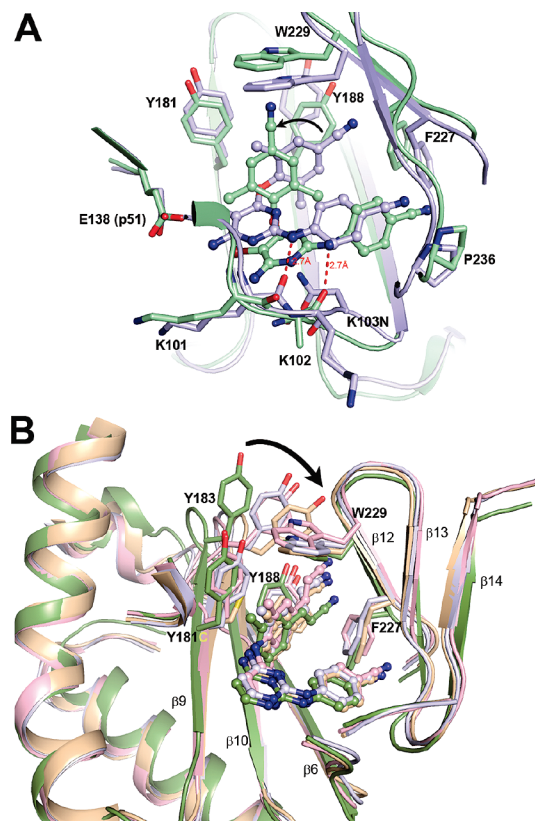

Figure 4. (A) Alignment of K103N RT with TMC125 presented in this report (light blue) and PDB code 1SV5 (green). The rmsd in aligned protein Cα atoms is 1.1 Å. The dimethylcyanophenyl group is rotated ∼50° between structures. The hydrogen bond between the secondary amine to the protein backbone is shown with a dashed line. (B) Comparison of the WT-TMC278 structure to crystal structures derived with an engineered RT. WT-TMC278 is shown in dark green, 2ZD1 (WT-TMC278) in gray, 3BGR (K103N/Y181C-TMC278) in tan, 2ZE2 (L100I/K103N-TMC278) in light red. Residues 94−100 are omitted from the backbone trace for clarity.

chain.[10] It is unclear what effect the engineered RT has on the position of this loop and the orientation of the acrylonitrile.

TMC125 and TMC278 have a high genetic barrier to forming resistance mutations and generally require multiple mutations to confer significant resistance.[4,6,8] Neither drug shows significant resistance to common point mutations K103N, Y181C, G190A, L100I, V179I, and Y188L which line the NNRTI pocket. Recently, E138R was identified as a

novel resistance-associated mutation to TMC278.[8] E138 is part of the p51 subunit that lines part of the NNIBP (Figure 2C). The pyrimidine core is found near E138, and the longer basic E138R side chain may have a negative effect on pyrimidine binding. Notably, both drugs maintain activity against the clinically relevant point mutation K103N. In these structures, the K103N mutation does not alter the binding mode of either compound (Table 2). A previous apo crystal structure of K103N mutant RT revealed an extra hydrogen bond within the collapsed NNIBP between N103 and Y183 side chains.[14] In order for an NNRTI to be effective, it must overcome the penalty for breaking this hydrogen bond and enter the NNIBP. However, the length and angle of this hydrogen bond are not ideal and thus the importance of overcoming this interaction for an NNRTI is debatable.[1] Compensatory interactions with K103N by an NNRTI may also aid toward a flat resistance profile. For example, recent crystal structures of GW4511 show that this compound is able to form extra van der Waals contacts with the K103 amide side chain.[13] In this report, van der Waals interactions are observed between the N103 side chain and TMC125 and TMC278. In the K103N RT TMC125 structure, the N103 amide located below the aniline linker possibly forms a favorable interaction at 3.3 Å between the aniline and amide. This interaction may help to reinforce the conserved hydrogen bond between the aniline linker and K101 carbonyl. In the K103N RT TMC278 structure, this interaction may have additional benefit. The hydrogen bond distances are slightly closer between the aniline linker to the amide side chain (3.1 Å) K101 carbonyl (3.0 Å). Perhaps these extra interactions with N103 help compensate for the loss of the Y188 hydrogen bond in the apo state.

Experimental Section

Protein Crystallization. HIV-1 RT from the HXB2D virus was expressed and purified in a manner described previously.[15] A detailed description of the purification of HIV-1 RT for crystallization is available in the Supporting Information. Crystal trials were initiated with protein and inhibitor concentrations at 20 mg/mL and 400 μM, respectively, by hanging drop vapor diffusion at 20 °C. To obtain cocrystals with TMC125 and TMC278, previously grown cocrystals with nevirapine were used as seeds. The crystals with nevirapine were easily obtained by mixing 2 μL of RT/nevirapine solution with 2 μL of mother liquor containing 1.4 M $(NH_4)_2SO_4$, 100 mM cacodylate, pH 6.5, and 30 mM Na malonate. These crystals were used as seeds by removing one crystal and placing in fresh mother liquor. The crystal was crushed with a metal probe, and the seed solution was diluted into 50 μL of mother liquor. A small amount of this solution was next combined with fresh protein/inhibitor complex solution with TMC125 or TMC278. This procedure produced small cocrystals of RT with TMC125 and TMC278. This dilution seeding process was repeated once more using the respective TMC125 or TMC278 crystals as starter seeds to produce larger crystals for data collection.

Supporting Information Available: Experimental procedures for protein expression, purification, data collection, and structure determination. This material is available free of charge via the Internet at http://pubs.acs.org.

References

(1) Ren, J.; Stammers, D. K. Structural basis for drug resistance mechanisms for non-nucleoside inhibitors of HIV reverse transcriptase. *Virus Res.* **2008**, *134*, 157–170.

(2) Tambuyzer, L.; Azijn, H.; Rimsky, L. T.; Vingerhoets, J.; Lecocq, P.; Kraus, G.; Picchio, G.; de Bethune, M. P. Compilation and prevalence of mutations associated with resistance to non-nucleoside reverse transcriptase inhibitors. *Antiviral Ther.* **2009**, *14*, 103–109.

(3) Johnson, L. B.; Saravolatz, L. D. Etravirine, a next-generation nonnucleoside reverse-transcriptase inhibitor. *Clin. Infect. Dis.* **2009**, *48*, 1123–1128.

(4) Andries, K.; Azijn, H.; Thielemans, T.; Ludovici, D.; Kukla, M.; Heeres, J.; Janssen, P.; De Corte, B.; Vingerhoets, J.; Pauwels, R.; de Bethune, M. P. TMC125, a novel next-generation nonnucleoside reverse transcriptase inhibitor active against nonnucleoside reverse transcriptase inhibitor-resistant human immunodeficiency virus type 1. *Antimicrob. Agents Chemother.* **2004**, *48*, 4680–4686.

(5) Goebel, F.; Yakovlev, A.; Pozniak, A. L.; Vinogradova, E.; Boogaerts, G.; Hoetelmans, R.; de Bethune, M. P.; Peeters, M.; Woodfall, B. Short-term antiviral activity of TMC278—a novel NNRTI—in treatment-naive HIV-1-infected subjects. *AIDS* **2006**, *20*, 1721–1726.

(6) Janssen, P. A.; Lewi, P. J.; Arnold, E.; Daeyaert, F.; de Jonge, M.; Heeres, J.; Koymans, L.; Vinkers, M.; Guillemont, J.; Pasquier, E.; Kukla, M.; Ludovici, D.; Andries, K.; de Bethune, M. P.; Pauwels, R.; Das, K.; Clark, A. D., Jr.; Frenkel, Y. V.; Hughes, S. H.; Medaer, B.; De Knaep, F.; Bohets, H.; De Clerck, F.; Lampo, A.; Williams, P.; Stoffels, P. In search of a novel anti-HIV drug: multidisciplinary coordination in the discovery of 4-[[4-[[4-[(1*E*)-2-cyanoethenyl]-2,6-dimethylphenyl]amino]-2- pyrimidinyl]amino]-benzonitrile (R278474, rilpivirine). *J. Med. Chem.* **2005**, *48*, 1901–1909.

(7) Two phase III clinical trials ongoing: http://clinicaltrials.gov.

(8) Azijn, H.; Tirry, I.; Vingerhoets, J.; de Bethune, M. P.; Kraus, G.; Boven, K.; Jochmans, D.; Van Craenenbroeck, E.; Picchio, G.; Rimsky, L. T. TMC278, a next-generation nonnucleoside reverse transcriptase inhibitor (NNRTI), active against wild-type and NNRTI-resistant HIV-1. *Antimicrob. Agents Chemother.* **2010**, *54*, 718–727.

(9) Das, K.; Clark, A. D., Jr.; Lewi, P. J.; Heeres, J.; De Jonge, M. R.; Koymans, L. M.; Vinkers, H. M.; Daeyaert, F.; Ludovici, D. W.; Kukla, M. J.; De Corte, B.; Kavash, R. W.; Ho, C. Y.; Ye, H.; Lichtenstein, M. A.; Andries, K.; Pauwels, R.; De Bethune, M. P.; Boyer, P. L.; Clark, P.; Hughes, S. H.; Janssen, P. A.; Arnold, E. Roles of conformational and positional adaptability in structure-based design of TMC125-R165335 (etravirine) and related non-nucleoside reverse transcriptase inhibitors that are highly potent and effective against wild-type and drug-resistant HIV-1 variants. *J. Med. Chem.* **2004**, *47*, 2550–2560.

(10) Das, K.; Bauman, J. D.; Clark, A. D., Jr.; Frenkel, Y. V.; Lewi, P. J.; Shatkin, A. J.; Hughes, S. H.; Arnold, E. High-resolution structures of HIV-1 reverse transcriptase/TMC278 complexes: strategic flexibility explains potency against resistance mutations. *Proc. Natl. Acad. Sci. U.S.A.* **2008**, *105*, 1466–1471.

(11) Bauman, J. D.; Das, K.; Ho, W. C.; Baweja, M.; Himmel, D. M.; Clark, A. D., Jr.; Oren, D. A.; Boyer, P. L.; Hughes, S. H.; Shatkin, A. J.; Arnold, E. Crystal engineering of HIV-1 reverse transcriptase for structure-based drug design. *Nucleic Acids Res.* **2008**, *36*, 5083–5092.

(12) Lindberg, J.; Sigurdsson, S.; Lowgren, S.; Andersson, H. O.; Sahlberg, C.; Noreen, R.; Fridborg, K.; Zhang, H.; Unge, T. Structural basis for the inhibitory efficacy of efavirenz (DMP-266), MSC194 and PNU142721 towards the HIV-1 RT K103N mutant. *Eur. J. Biochem.* **2002**, *269*, 1670–1677.

(13) Ren, J.; Chamberlain, P. P.; Stamp, A.; Short, S. A.; Weaver, K. L.; Romines, K. R.; Hazen, R.; Freeman, A.; Ferris, R. G.; Andrews, C. W.; Boone, L.; Chan, J. H.; Stammers, D. K. Structural basis for the improved drug resistance profile of new generation benzophenone non-nucleoside HIV-1 reverse transcriptase inhibitors. *J. Med. Chem.* **2008**, *51*, 5000–5008.

(14) Hsiou, Y.; Ding, J.; Das, K.; Clark, A. D., Jr.; Boyer, P. L.; Lewi, P.; Janssen, P. A.; Kleim, J. P.; Rosner, M.; Hughes, S. H.; Arnold, E. The Lys103Asn mutation of HIV-1 RT: a novel mechanism of drug resistance. *J. Mol. Biol.* **2001**, *309*, 437–445.

(15) White, K. L.; Margot, N. A.; Ly, J. K.; Chen, J. M.; Ray, A. S.; Pavelko, M.; Wang, R.; McDermott, M.; Swaminathan, S.; Miller, M. D. A combination of decreased NRTI incorporation and decreased excision determines the resistance profile of HIV-1 K65R RT. *AIDS* **2005**, *19*, 1751–1760.